ROYAL SOCIETY
OF CHEMISTRY

EDGE ARTICLE

Check for updates

Photon upconversion with indium phosphide quantum dots enables high-energy photoreactions using visible light

Indra Narayan Chakraborty,†[a] Adhra S. Sury, [ID] †[a] Aman Chaturvedi,[a] Kaixing Wang,[b] Ankit Dhankhar, [ID] [a] Pankaj Mandal, [ID] [a] Benjamin Dietzek-Ivanšić*[bc] and Pramod P. Pillai [ID] *[a]

Photochemical reactions that rely on high-energy photons are limited by low solar abundance in the UV region and undesired photodecomposition. Photon upconversion processes, particularly triplet–triplet annihilation-based upconversion (TTA-UC), provide an alternate pathway to enable the use of low-energy, abundant visible and near-infrared (NIR) light for chemical transformations that typically require high-energy UV light. In this context, quantum dot (QD)-sensitized TTA-UC systems offer distinct advantages with respect to a larger anti-Stokes shift, enhanced upconversion quantum yield, and superior photostability. However, the successful application of QD-sensitized upconversion energy in photocatalysis remains limited, especially for high-energy reactions requiring UV-active catalysts. Here, we report the use of upconversion energy from a QD-sensitized TTA-UC system in performing a high-energy-driven dehalogenation reaction with visible light. Indium phosphide (InP) QDs are used as the sensitizer and diphenylanthracene (DPA) as the annihilator molecule, which gave a green-to-blue TTA-UC with a normalized upconversion quantum yield of $\sim$8.2% and an apparent anti-Stokes shift of 0.55 eV. The upconversion energy from the InP QD-sensitized TTA-UC system is effectively used to drive a photoredox C–C coupling reaction *via* the dehalogenation of substituted aryl halides in excellent yields. TTA-UC is the sole driving force for this photoredox reaction, as the required potential is beyond the maximum achievable redox potential of InP-QDs. Further, the scope of the QD-sensitized TTA-UC system is extended towards the radical polymerization of methyl methacrylate (MMA), resulting in the production of industrially important polymethyl methacrylate (PMMA). Our work overcomes key limitations of traditional UV-based photochemistry and introduces a sustainable, low-energy pathway for enabling high-energy transformations.

Introduction

The abundance of visible and near-infrared (NIR) light in the solar spectrum has made them ideal irradiation sources for the solar synthesis of valuable chemicals and materials.[1] However, its potential is often limited by the thermodynamic limits set by the maximum energy of visible-light photons.[2] In this direction, photon upconversion processes provide an alternative pathway by using the cumulative energy input of two or more lower-energy photons to generate higher-energy photons.[3] Such strategies enable the use of low-energy, abundant visible and near-infrared (NIR) light for chemical transformations that typically require high-energy UV light.[4] Triplet–triplet annihilation-based upconversion (TTA-UC) is one such pathway to generate higher-energy photons using a sensitizer and an annihilator molecule.[5] The TTA process involves a Dexter-type energy transfer from the triplet-state of the photosensitizer to the triplet-state of the annihilator molecule, which further undergoes the annihilation process to form a high-energy singlet-state of the annihilator molecule.[5–7] In addition to the photon emission from the upconverted state, the electrons in the high-energy singlet states can be extracted for photoredox transformations.[8–10] In this way, chemical reactions requiring higher potentials corresponding to UV light can be carried out with visible- or NIR-light excitation.[8–12] This has led to the development of a library of TTA-UC systems involving organic chromophores, metal complexes, and other solar absorbers as sensitizers.[13] Quantum dot (QD)-based sensitizers are the latest addition to TTA-UC as they offer an additional advantage of mixed singlet and triplet character of the excited states arising

[a]*Department of Chemistry, Indian Institute of Science Education and Research (IISER), Dr Homi Bhabha Road, Pune - 411 008, India. E-mail: pramod.pillai@iiserpune.ac.in*

[b]*Leibniz Institute of Photonic Technology, Albert Einstein-Strasse 9, 07745, Jena, Germany*

[c]*Leibniz Institute of Surface Engineering, Permoserstrasse 15, 04318, Leipzig, Germany. E-mail: benjamin.dietzek-ivansic@iom-leipzig.de*

† These authors contributed equally to this work.

from the strong spin–orbit coupling. This minimizes the energy loss due to intersystem crossing (ISC).[14–19] Accordingly, QD-sensitized TTA-UC systems have been developed in recent years with high quantum yield and photon energy gain.[14–28] However, the use of QD-sensitized upconversion energy in photocatalysis has been limited, when compared to molecular-sensitized UC systems.[29] To the best of our knowledge, only two examples have been reported to date, wherein NIR-to-visible-light upconversion energy was used in a photoredox reaction. Liang *et al.* performed a visible-light-driven reaction under NIR-light excitation using a Zn-doped CuInSe$_2$ QD-sensitized TTA-UC system.[27] More recently, Jiang *et al.* developed a PbS QDs-based NIR-II to visible TTA-UC system to demonstrate a photo-polymerization reaction using 1064 nm irradiation.[28] As it is clear from the literature, immediate efforts are required to harness QD-sensitized upconversion energy for high-energy-demanding reactions typically requiring UV-active catalysts, under visible- or NIR-light excitation. Achieving this task is essential to expand the applicability of QD-sensitized TTA-UC methodology across the entire UV-NIR spectrum, thereby widening the scope of photoredox reactions.
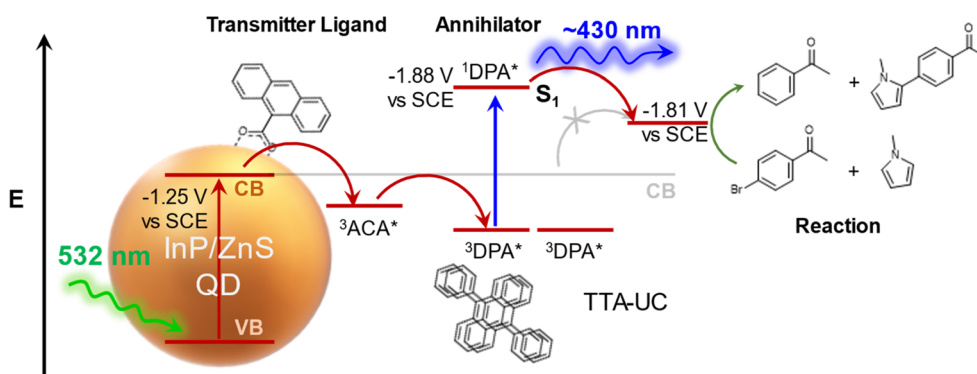
In this work, we used the upconversion energy from a QD-sensitized TTA process to perform a UV-light-driven photo-redox reaction under visible-light excitation. The system comprises environmentally friendly InP/ZnS QDs as the sensitizer, 9-anthracene carboxylic acid (ACA) as the transmitter ligand, and diphenylanthracene (DPA) as the annihilator molecule. Femtosecond transient absorption studies confirmed the triplet energy transfer from the InP/ZnS QDs to the ACA ligand, which was subsequently transmitted to the DPA annihilator. This cascade of energy transfer resulted in green-to-blue TTA-UC with ~8.2% normalized upconversion quantum yield (UCQY) and an apparent anti-Stokes shift of 0.55 eV. The process led to the generation of high-energy DPA singlet states (^{1}DPA*), which were further harnessed to catalyze UV-driven dehalogenation and C–C coupling reactions in excellent yields (85%) (Scheme 1). Typically, DPA requires UV excitation to photocatalyse the dehalogenation and C–C coupling reactions in substituted aryl halides. However, the continuous illumination of high-energy UV light often results in photodegradation

of the aryl halides and other species involved in the reaction. With the help of InP/ZnS QD-sensitized TTA-UC, the catalytic activity of DPA was triggered using ~532 nm excitation. Detailed spectroscopic analyses gave valuable insights into the InP/ZnS QD-sensitized green-to-blue TTA-UC, along with the underlying reaction pathway in the photoredox catalysis. The versatility of the InP/ZnS QD-sensitized TTA-UC-driven photocatalysis was proved by successfully performing a UV-light-driven radical polymerization of acrylates under visible-light excitation. Our work introduces QD-based sensitizers to the club of traditional molecular sensitizers for driving high-energy UV-driven chemical synthesis with low-energy visible light *via* TTA-UC.

Results and discussion

Design of InP/ZnS QD-based sensitizer

In the present study, we selected quantum dots (QDs) as the sensitizer due to their strong optoelectronic properties, such as large absorption cross-section, easy tunability of band positions, high photostability, and the presence of spin-mixed energy states—a crucial factor for minimizing the energy loss in the TTA process.[14–19,30–32] (see Section 3, Table S1 of SI for state of the art on QD-sensitized TTA-UC.) Among the wide range of QDs available, our choice of sensitizer was InP-based QDs because of the following reasons: (i) InP QDs are environmentally friendly as they are free of any toxic-metal ions, which enhances the translational and sustainability prospects,[33–35] and (ii) the charge storage in InP QDs is for a longer time compared to conventional II–VI QDs ($\tau = 25.5 \pm 0.4$ min for InP and $\tau = 7.2 \pm 0.4$ min for CdS).[36] This is attributed to weak coulombic interaction between holes and electrons in III–V InP QDs due to the more covalent nature of bonding and smaller effective mass of charge carriers.[35–37] Accordingly, InP-based QDs have emerged as a promising light-harvester in several areas of solar energy research, including photocatalysis.[38–40] Very recently, Wu and co-workers used InP/ZnSe/ZnS core/shell QDs as sensitizers for achieving green-to-blue TTA-UC.[24] Inspired by these reports and along with our own group's prior research on InP QDs, we used InP/ZnS core/shell QD as a sensitizer in the design of the desired

Scheme 1 Schematic representation of the TTA-UC process with ACA-capped InP/ZnS QDs as sensitizers and DPA as annihilators. The upconversion energy from the InP-based QD-sensitized TTA-UC system was used to drive the dehalogenation of substituted aryl halides, which typically require a potential exceeding the maximum achievable redox potential of InP/ZnS QDs.

green-to-blue TTA-UC system. Oleylamine-capped InP/ZnS QDs with a diameter of ~3.7 nm were synthesized, using a previously reported procedure.[41] The as-synthesized InP/ZnS QDs exhibited the first excitonic peak at ~500 nm and a PL emission peak at ~550 nm, with an average PL decay lifetime of ~55 ns and an excellent absolute PLQY of ~75% in toluene (Fig. S1).

Triplet–triplet energy transfer (TTEnT) from InP/ZnS QDs

Bulkier ligands (oleylamine) on the surface of QDs can hinder the direct transfer of energy from the QDs to the annihilator molecules. Thus, a transmitter ligand is often used to facilitate the energy cascade between the QDs and the annihilator, thereby enhancing the overall upconversion quantum yield.[42,43] Accordingly, the InP/ZnS QDs were functionalized with 9-anthracenecarboxylic acid (ACA), a transmitter ligand, using a suitable ligand exchange protocol (Fig. 1a).[14,24] The triplet-state energy (E_T) of ACA is at 1.83 eV,[24] which lies between the band gap of InP/ZnS QDs (2.29 eV) and the E_T of annihilator DPA (1.77 eV),[24] enabling the efficient extraction and transfer of triplet energy from the photoexcited QDs to the annihilator DPA (Fig. S2). The presence of the characteristic sharp absorption features of ACA below 400 nm, along with the retention of the first excitonic peak of the InP/ZnS QDs at ~500 nm, confirms the successful functionalization of ACA on the QD surface (Fig. 1b). As expected, significant quenching in the PL of InP/ZnS QDs with ~80% efficiency was observed upon functionalization with the transmitter ligand ACA (Fig. 1c). Time-resolved PL quenching experiments further confirm an efficient TTEnT from the InP/ZnS QDs to the low-lying triplet-state of the ACA molecules with a TTEnT time constant of 14.4 ns and efficiency

of ~80% (Fig. 1d, Table S2). To confirm that the energy transfer step solely follows a TTEnT pathway, a PL quenching experiment was performed with another polyaromatic carboxylate ligand with a triplet energy level higher than the band gap of InP/ZnS QDs (1-naphthoic acid, NCA, with E_T = 2.60 eV, Fig. 1e).[24] Interestingly, negligible quenching of the QD PL was observed in both steady-state as well as time-resolved PL experiments upon NCA functionalization (Fig. S3a and b). This study overrules both the possibilities of surface trap states induced upon ligand exchange and the involvement of any alternate energy/charge transfer mechanism, other than TTEnT, in the PL quenching of InP/ZnS QD by ACA (Fig. S3c).

To gain further insights into the TTEnT process, femtosecond transient absorption (fs-TA) studies were performed. The fs-TA spectra of InP/ZnS QDs and InP/ZnS QD–ACA following 500 nm excitation are shown in Fig. 2a and b, respectively. The prominent depletion signal at ~500 nm reflects the ground-state bleach (GSB) of the QD first excitonic band. The GSB feature recovers at a significantly accelerated rate in surface-functionalized InP/ZnS QD–ACA as compared to only InP/ZnS QDs (Fig. 2c). The accelerated recovery is also accompanied by the growth of an absorptive feature corresponding to the $T_1 \rightarrow T_n$ transition of the triplet states of ACA at ~430 nm (Fig. 2b inset and S4).[24] These observations provide direct evidence for the TTEnT from the InP/ZnS QDs to the ACA ligands.

InP/ZnS QD sensitized green-to-blue TTA-UC

With the InP/ZnS-ACA system showing an efficient triplet sensitization of ACA by InP/ZnS QDs, the next step was to
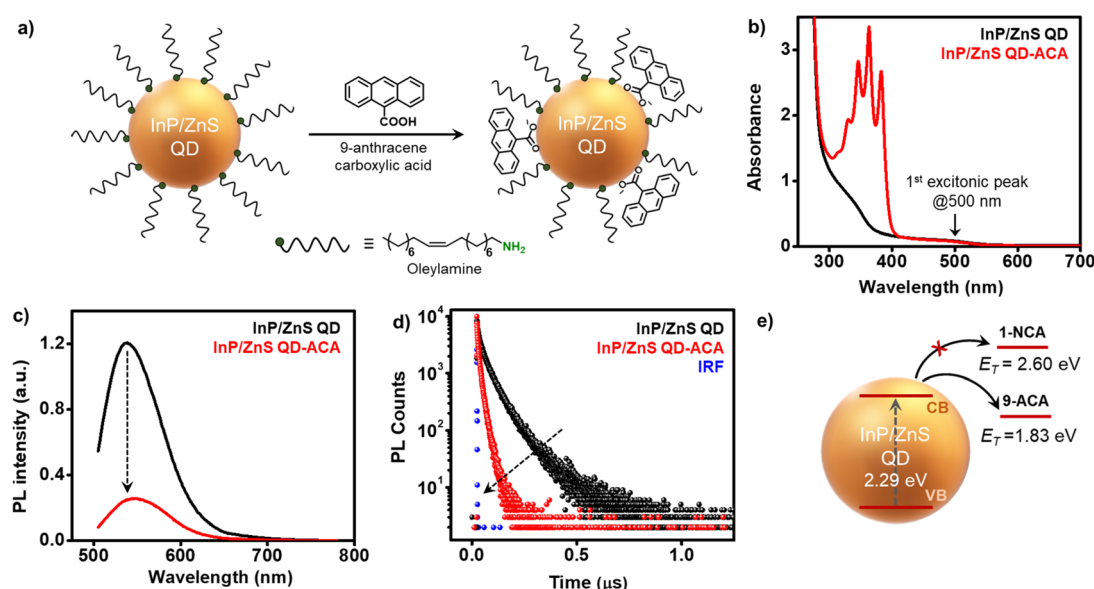

Fig. 1 (a) Schematic representation of the surface functionalization of OAm-capped InP/ZnS QDs with ACA, using a ligand exchange protocol. (b) Absorption spectra of InP/ZnS QDs before and after the ligand exchange with ACA, showing the characteristic absorption peaks of ACA molecules below 400 nm. The corresponding (c) steady-state and (d) time-resolved PL spectra of InP/ZnS QDs, showing significant quenching after the surface functionalization with ACA molecules. (e) Schematics showing the successful TTEnT from the photoexcited InP/ZnS QDs to the low-lying triplet state of the surface-bound ACA. A TTEnT from the photoexcited InP/ZnS QDs to the triplet state of NCA is thermodynamically not feasible, which was observed in the experiment as well (Fig. S3).
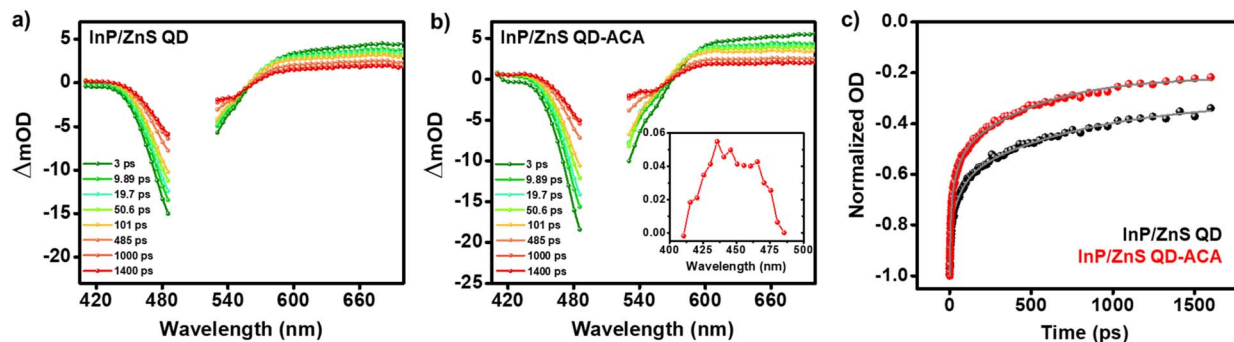
Fig. 2 fs-TA spectra at indicated time delays upon 500 nm excitation of (a) InP/ZnS QDs and (b) InP/ZnS QD-ACA. Inset of (b) shows the absorption feature of ^{3}ACA* at ~430 nm obtained by subtracting the normalized spectra corresponding to 1400 ps and 3 ps time delays. (c) Kinetics of the GSB bleach recovery of InP/ZnS QDs with and without ACA ligands.

introduce the annihilator DPA into the system to achieve the desired TTA-UC process. As shown in Fig. 3a, the E_T of DPA is 1.77 eV, which is lower than that of ACA ($E_T = 1.83$ eV), allowing further TTEnT from the sensitized surface-bound ^{3}ACA*. The 532 nm excitation of the mixture (InP/ZnS QD–ACA + DPA) clearly produces a blue emission, corresponding to the decay of the first excited singlet state of DPA (captured using a 500 nm short-pass filter, as shown in Fig. 3b), confirming an effective TTA-UC process. The collected spectrum showed an apparent anti-Stokes shift (Δ_{as}) of 0.55 eV, estimated from the energy

difference between the λ_{max} of the upconversion emission signal and the excitation wavelength of the laser source (Fig. 3c). The upconversion emission signal also overlaps well with the fluorescence spectrum of DPA recorded by the direct excitation with $\lambda_{ex} = 365$ nm (inset of Fig. 3c). This confirms that the observed emission in the InP/ZnS-ACA-DPA mixture is indeed originating from the ^{1}DPA* molecule generated via the TTA-UC. The intensity of the UC signal increased steadily with the increase in the power density of the laser excitation (Fig. 3d; see Fig. S5 for beam diameter calculation). The integrated values of
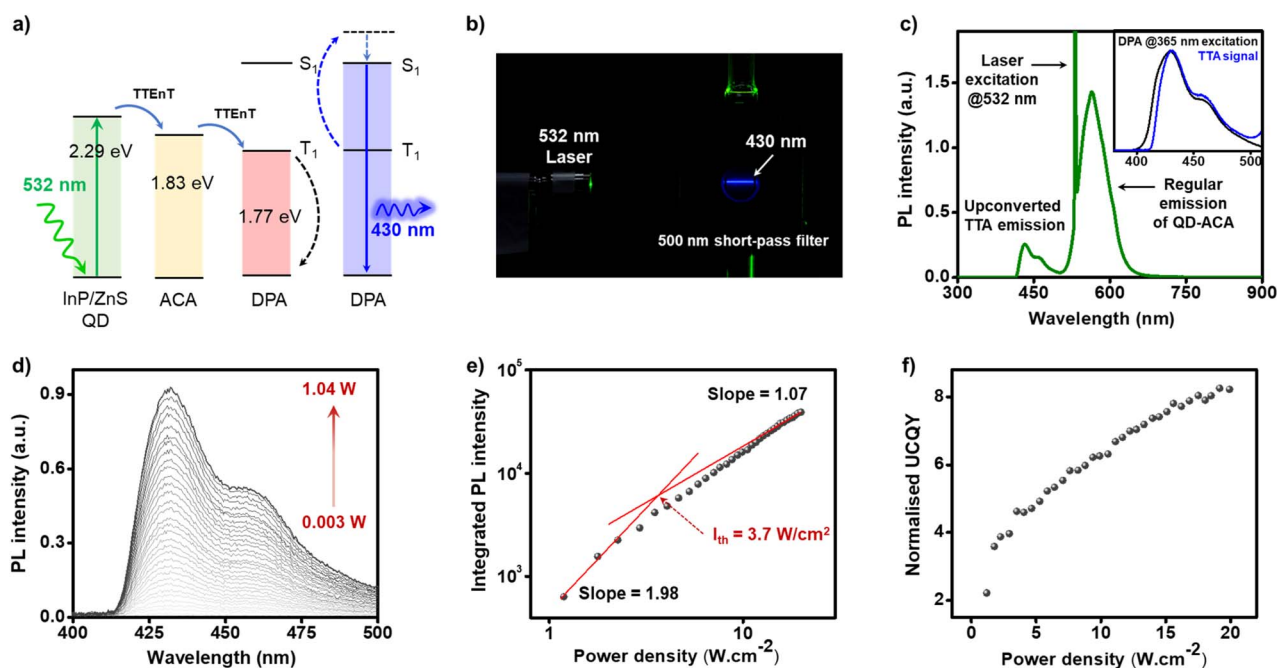

Fig. 3 InP/ZnS QD-sensitized TTA-UC system and the characterization of the TTA-UC signal. (a) A schematic representation of the TTA-UC process containing InP/ZnS QD as the sensitizer, ACA as the triplet-transmitter ligand, and DPA as the annihilator. (b) The optical photograph showing the bright blue upconversion signal from the cuvette (through a 500 nm short-pass filter) containing a solution of InP/ZnS-ACA and DPA, upon excitation with a 532 nm diode laser. (c) The overall PL spectrum of the TTA-UC signal without any filter, showing the upconverted signal (λ_{max} ~430 nm), the laser excitation (λ_{max} ~532 nm), and the direct PL of the InP/ZnS QDs (λ_{max} ~550 nm). Inset shows an overlap between the TTA-UC signal and the fluorescence of DPA (obtained by the direct excitation of DPA at ~365 nm), confirming that the final emission arises from DPA. The concentration of DPA was 16 mM in these studies. (d) The intensity of the upconversion signal increases with the increase in the power density of the laser source. (e) Log–log plot of the integrated UC intensity vs. laser power density showing the transition from quadratic to linear regime with I_{th} value of 3.7 W cm^{-2}. (f) The calculated TTA-UC QY plotted as a function of the laser power density.

the UC peak under increasing laser power density first increased quadratically, then changed to linear increase after a cross-over point (Fig. 3e). This cross-over point, defined as the TTA-UC threshold intensity (I_{th}), was observed to be ~3.7 W cm^{-2} under our experimental conditions (Fig. 3e). Below this point, at lower power densities, the concentration of triplet-sensitized DPA ([^{3}DPA*]) remains low, favoring spontaneous decay of [^{3}DPA*] over TTA. However, above the I_{th} value, the [^{3}DPA*] becomes sufficiently high, making TTA the dominant decay pathway, which results in a linear increase in the TTA-UC intensity with respect to the excitation power density. This leads to a shift in the slope of a double logarithmic plot of the integrated UC PL intensity *vs.* power density from ~2 to ~1 above the I_{th} point. All these observations are in accordance with the signatures of a TTA-UC process.[44] Next, the QY of the TTA-UC process was calculated using rhodamine-6G as a reference dye. The normalized UCQY increased with excitation intensity, finally reaching a plateau of constant QY at higher incident power densities (Fig. 3f). Among the different concentrations of QD–ACA complex and annihilator studied, a maximum UCQY of ~8.2% was obtained under experimental conditions containing 0.2 µM of InP/ZnS-ACA and 16 mM DPA in an Ar-purged toluene solution (Fig. 3f and S6). It must be noted here that QD-sensitized TTA-UC systems often suffer from reabsorption losses since the QDs can themselves absorb the upconverted emission because of their broadband absorption, thereby reducing the measured UCQY.[15–19,27] One effective strategy to mitigate this loss is to directly utilize the singlet excited state of the annihilator for photoredox transformations, which is the main objective of the present work.

Photoredox catalysis using TTA-UC

The optimized TTA-UC process was further applied in high-energy photoredox transformations that occur at potentials beyond the redox limit of InP/ZnS QDs. For that, we selected the dehalogenation of aryl bromide substrates followed by the C–C coupling as the model reaction (Fig. 4a). The redox potential required for the dehalogenation of 4-bromoacetophenone (E_{red} = −1.81 V *vs.* SCE)[9] is beyond the redox limit of the InP/ZnS QD (E_{CB} = −1.25 V *vs.* SCE; Fig. S7; see Section 5 of SI for details). In a typical reaction, 4-bromoacetophenone (1 eq., 0.25 mmol), *N*-methylpyrrole (50 eq., 12.5 mmol), and DIPEA (150 µL, 0.85 mmol) were mixed with a solution containing 16 mg (0.048 mmol, 20 mol%) of DPA and 4 µM of InP/ZnS-ACA in a 1 : 1 benzene : DMSO solvent mixture in a long-neck cuvette. The system was purged with Ar for 15 min, after which the sealed cuvette was irradiated with a 1 W, 532 nm continuous-wave laser beam focused on the cuvette wall. Interestingly, after 12 h of irradiation, excellent conversion (~85%) of 4-bromo-acetophenone was observed, with the yields of the dehaloge-nation and C–C-coupled products estimated to be ~34% and ~47%, respectively (entry 1 in Fig. 4b, and S8–S10). Importantly,

a) Reaction scheme

Bromoacetophenone (0.25 mmol, 1 eq.) + N-methylpyrrole (12.5 mmol, 50 eq.) → [InP/ZnS-ACA + DPA; DIPEA, 532 nm Laser, Solvent, rt, 12 h; 0.0048 mol% QD] → Acetophenone (A) + C-C coupled product (B)

b) Control studies

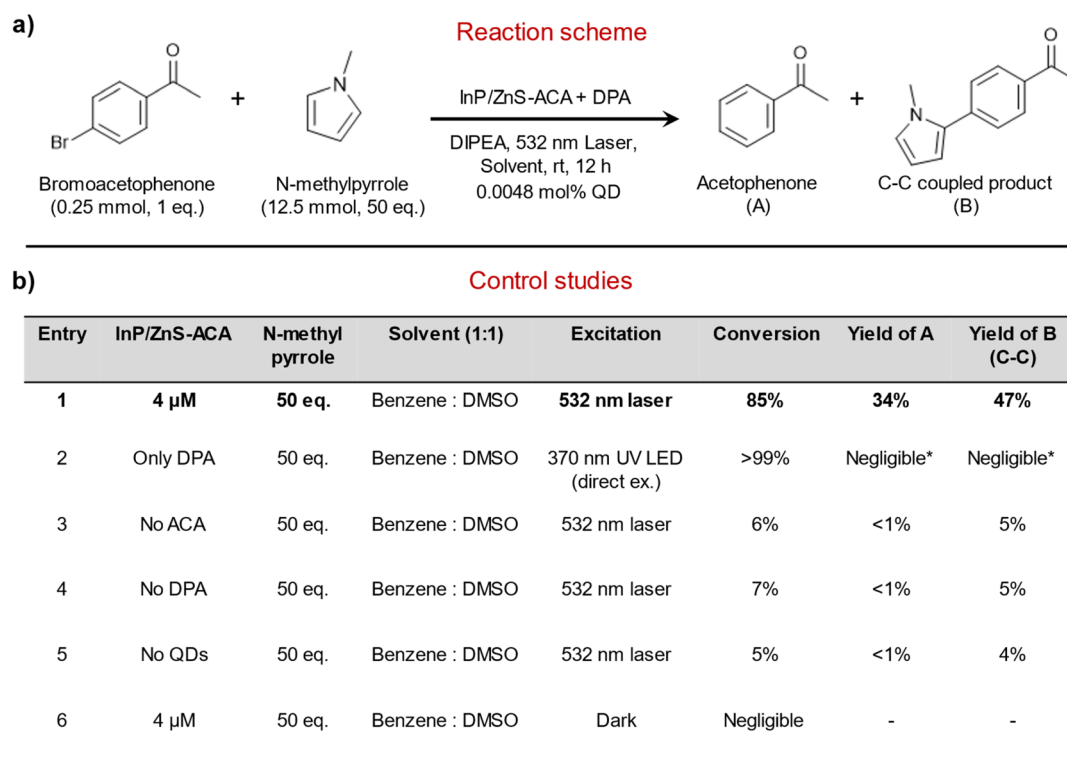| Entry	InP/ZnS-ACA	N-methyl pyrrole	Solvent (1:1)	Excitation	Conversion	Yield of A	Yield of B (C-C)
1	**4 µM**	**50 eq.**	Benzene : DMSO	**532 nm laser**	**85%**	**34%**	**47%**
2	Only DPA	50 eq.	Benzene : DMSO	370 nm UV LED (direct ex.)	>99%	Negligible*	Negligible*
3	No ACA	50 eq.	Benzene : DMSO	532 nm laser	6%	<1%	5%
4	No DPA	50 eq.	Benzene : DMSO	532 nm laser	7%	<1%	5%
5	No QDs	50 eq.	Benzene : DMSO	532 nm laser	5%	<1%	4%
6	4 µM	50 eq.	Benzene : DMSO	Dark	Negligible	-	-

Fig. 4 Photoredox catalysis using InP/ZnS QD-sensitized TTA-UC system. (a) The optimized photocatalytic redox reaction scheme for the dehalogenation of 4-bromoacetophenone and C−C coupling reaction between 4-bromoacetophenone and *N*-methylpyrrole. (b) A table showing the optimized condition as well as other control experiments under different reaction conditions. All these experiments confirm the sole role of the TTA-UC process in enabling the photocatalytic redox reaction with visible light (*The negligible yields obtained with direct excitation of DPA catalyst could be attributed to photodegradation due to prolonged UV irradiation.).

a conversion yield of >99% was observed when the same reaction was performed under ~370 nm UV irradiation for 12 h, with DPA as the sole photocatalyst (entry 2 in Fig. 4b and S11a). However, only negligible amounts of both C–C-coupled and dehalogenation products were formed, which could be attributed to the degradation of the reactants and products under prolonged UV excitation. This highlights the advantage of TTA-UC over direct UV excitation in photoredox reactions (see Fig. S12, Section 8 of SI for detailed experiments). A series of control experiments in the absence of either (i) QDs, (ii) DPA, (iii) ACA, or (iv) light gave negligible conversion yield, confirming that the photoredox reaction is solely driven by the TTA-UC process (Fig. 4b entries 3–6 and Fig. S11b–e). Thus, a reaction with high reduction potential (E_{red} for aryl radical is −1.81 V vs. SCE) was successfully carried out using a low-energy excitation, showcasing the power of the TTA-UC process.

Next, a plausible mechanism is presented based on the experimental data obtained and the literature reports (Fig. 5a). The singlet excited state of DPA (^{1}DPA*) (1), generated via InP/ZnS QD-sensitized TTA-UC, can undergo a reductive or oxidative quenching pathway to activate the C–Br bond in 4-bromoacetophenone (3) via the formation of DPA$^{•−}$ or DPA$^{•+}$, respectively. PL quenching experiments were performed to identify the pathway in the present study. In these experiments, DPA molecules were directly excited at 385 nm, and its fluorescence was monitored in the presence of either 3 or DIPEA (at the same ratio as in the reaction mixture). Minimal quenching of the DPA fluorescence was observed upon the addition of 3 (80

mM) to the DPA solution, confirming that the electron transfer from 1 (i.e., the oxidative quenching) is not the likely first step. On the other hand, upon the addition of DIPEA (300 mM) to the DPA solution, substantial quenching of the DPA fluorescence (~70%) was observed, confirming that reductive quenching is the first step in the photocatalytic process (Fig. 5b). The Stern–Volmer plot constructed from fluorescence quenching data confirms the superior PL quenching of DPA by DIPEA, further validating the reductive quenching pathway (Fig. 5c). The reductive quenching pathway results in the formation of DPA$^{•−}$ (2) and the DIPEA radical cation (DIPEA$^{•+}$). 2 then transfers its photoexcited electron to 1, generating 4-bromoacetophenone radical anion (4), which finally dissociates to form the aryl radical (5). The radical 5 can then get trapped by N-methyl pyrrole to yield the C–C-coupled product (6) or undergo a hydrogen atom transfer from the DIPEA$^{•+}$ to produce acetophenone (7). The dehalogenation of aryl halides in the presence of DIPEA is well-known to follow a radical-based pathway.[45] The formation of the C–C-coupled product 6 in a significant amount (~45%) further confirms that a radical-based pathway is involved in the present study as well.

Radical-mediated photopolymerization with TTA-UC process

The ability of the TTA-UC process to generate the radical under visible light excitation motivated us to use the aryl radical (5 in Fig. 5a) as an initiator for a photopolymerization reaction. We chose the radical polymerization of methyl methacrylate (MMA) to produce polymethyl methacrylate (PMMA). The radical
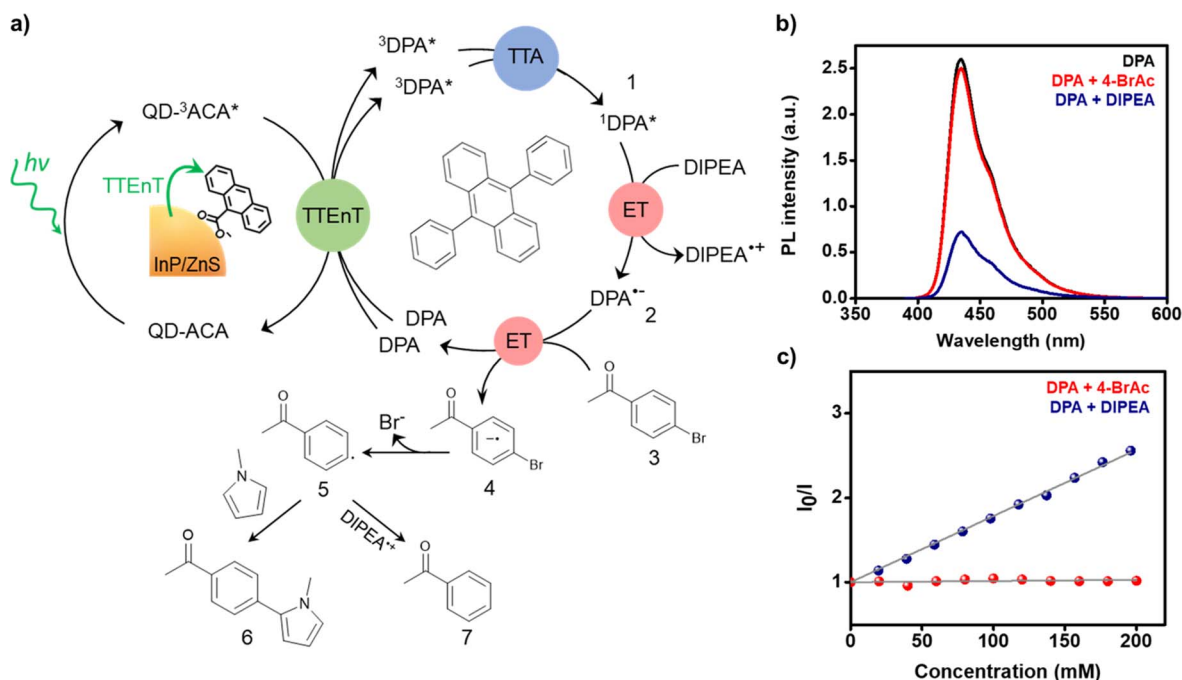

Fig. 5 (a) Schematic representation of the plausible mechanism of photocatalytic redox reaction driven by the upconversion energy generated from the InP/ZnS QD-sensitized TTA-UC process. ^{1}DPA* formed via the TTA-UC process participates in a series of charge transfer steps, which eventually lead to the formation of the aryl radical 5. (b) The photophysical studies show negligible quenching of the fluorescence of DPA in the presence of 4-bromoacetophenone; whereas a drastic quenching of DPA fluorescence in presence of DIPEA. (c) Stern–Volmer plot obtained from the relative fluorescence quenching of DPA in the presence of 4-bromoacetophenone and DIPEA. This confirms that the excited ^{1}DPA* first undergoes reductive quenching in the presence of DIPEA during the photocatalytic process.
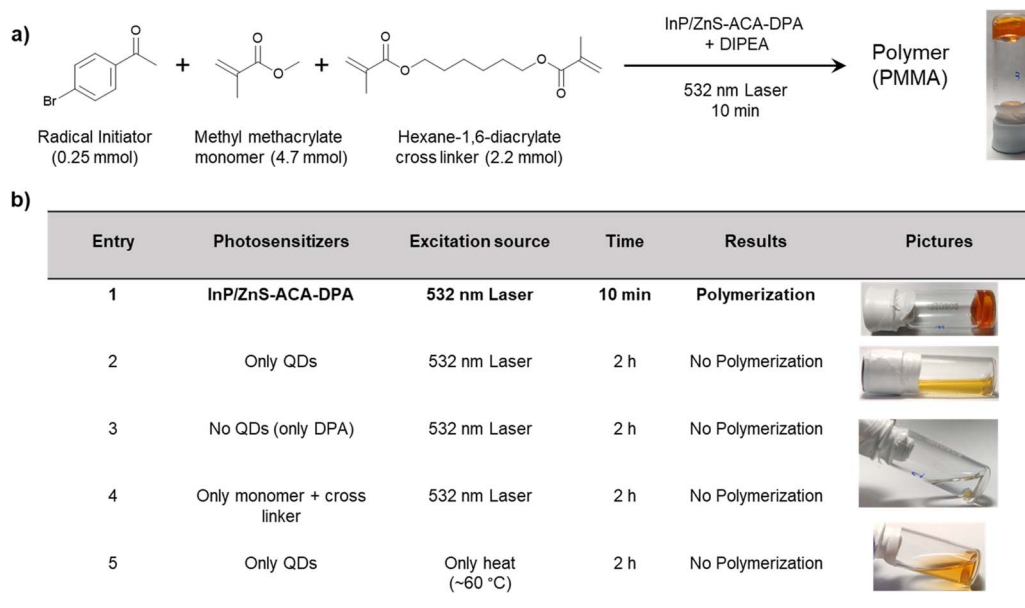
Fig. 6 Photopolymerization of MMA with InP QD-sensitized TTA-UC system. (a) Schematic representation of the optimized conditions for photopolymerization of MMA with the InP QD-sensitized TTA-UC system. (b) A table summarizing the optimized conditions for the polymerization reaction, as well as the control experiments confirming the sole involvement of the InP/ZnS QD-sensitized TTA-UC process.

polymerization of MMA is conventionally carried out in presence of an initiator under high-energy UV light excitation.[46] Considering the wide range of applications of PMMA, shifting from a high-energy UV excitation to a lower-energy and more abundant visible-light excitation is a more sustainable approach to drive the polymerization of MMA. In this context, the suitability of the InP QD-sensitized TTA-UC system developed in the present study was tested. Within 10 min of irradiation with a 532 nm continuous-wave laser, the liquid reaction mixture turned into a solid polymer gel, as shown in Fig. 6a. Control experiments in the absence of either DPA or QDs or both showed no signs of polymerization, even when the irradiation was carried out for ~2 h (Fig. 6b, entries 2–4). Moreover, no signs of polymerization were observed under continuous heating of the reaction mixture for ~2 h at ~60 °C, confirming that TTA-UC is solely responsible for the photopolymerization (Fig. 6b, entry 5).

Conclusions

Our work showcases the potential of the InP QD-sensitized TTA-UC system in driving high-energy-driven chemical transformations with lower-energy excitations. Photophysical studies reveal the active involvement of a bimolecular annihilation process, with a green-to-blue UCQY of ~8.2% and an apparent anti-Stokes shift (Δ_{as}) of 0.55 eV. The upconversion energy from the InP QD-sensitized TTA-UC system was used to drive the photoactivation of substituted aryl-bromides under visible-light excitation, leading to the formation of corresponding dehalogenated and C–C-coupled products. An excellent conversion yield of ~85% was achieved in 12 h for the TTA-UC-triggered photoredox reaction. Further, the upconversion energy from

the InP QD-sensitized TTA-UC system was used to produce PMMA within 10 min of visible-light-driven radical polymerization of MMA. Thus, two UV-light-driven chemical reactions were efficiently performed with visible-light excitation by harnessing QD-sensitized upconversion energy. The introduction of QD-sensitized green-to-blue UC into chemical synthesis could promote the use of visible-light excitation for driving a wider set of chemical transformations that typically demand UV light excitation. Such approaches are essential to achieve more sustainability in chemical synthesis.

Author contributions

I. N. C. and A. S. S. prepared and characterized the InP/ZnS QDs. I. N. C. performed the TTA-UC and photocatalytic studies with the help of A. S. S. and A. D. A. C. and P. M. helped in the detection of TTA signal and beam diameter measurement. K. W. and B. D. -I. performed and helped in fs-TAS measurements and analysis. All authors contributed to the discussion, writing, and provided feedback on the manuscript. P. P. P. conceived the project and coordinated the research.

Conflicts of interest

There are no conflicts to declare.

Data availability

The article and supplementary information (SI, includes instrumentation, calculations, characterization of TTA components, corresponding studies related to TTEnT and TTA-UC process, cyclic voltammogram, and characterization of

products) contain data supporting the findings of the study. The corresponding author will provide appropriate source data upon reasonable request. Supplementary information is available. See DOI: **https://doi.org/10.1039/d5sc07232h**.

Acknowledgements

References

1 G. Ciamician, *Science*, 1912, **36**, 385–394.

2 F. Glaser, C. Kerzig and O. S. Wenger, *Angew. Chem., Int. Ed.*, 2020, **59**, 10266–10284.

3 J. Zhou, Q. Liu, W. Feng, Y. Sun and F. Li, *Chem. Rev.*, 2015, **115**, 395–465.

4 M. Uji, T. J. B. Zähringer, C. Kerzig and N. Yanai, *Angew. Chem., Int. Ed.*, 2023, **62**, e202301506.

5 T. N. Singh-Rachford and F. N. Castellano, *Coord. Chem. Rev.*, 2010, **254**, 2560–2573.

6 P. Bharmoria, H. Bildirir and K. Moth-Poulsen, *Chem. Soc. Rev.*, 2020, **49**, 6529–6554.

7 V. D. Andreeva, I. Regeni, T. Yang, A. Elmanova, M. Presselt, B. Dietzek-Ivansic and S. Bonnet, *J. Phys. Chem. Lett.*, 2024, **15**, 7430–7435.

8 M. Majek, U. Faltermeier, B. Dick, R. Pérez-Ruiz and A. von Wangelin, *Chem. Eur J.*, 2015, **21**, 15496–15501.

9 C. G. López-Calixto, M. Liras, V. A. de la Peña O'Shea and R. Pérez-Ruiz, *Appl. Catal. B Environ.*, 2018, **237**, 18–23.

10 B. D. Ravetz, A. B. Pun, E. M. Churchill, D. N. Congreve, T. Rovis and L. M. Campos, *Nature*, 2019, **565**, 343–346.

11 C. Kerzig and O. S. Wenger, *Chem. Sci.*, 2018, **9**, 6670–6678.

12 B. Pfund, D. M. Steffen, M. R. Schreier, M.-S. Bertrams, C. Ye, K. Börjesson, O. S. Wenger and C. Kerzig, *J. Am. Chem. Soc.*, 2020, **142**, 10468–10476.

13 L. Huang and G. Han, *Nat. Rev. Chem.*, 2024, **8**, 238–255.

14 Z. Huang, X. Li, M. Mahboub, K. M. Hanson, V. M. Nichols, H. Le, M. L. Tang and C. J. Bardeen, *Nano Lett.*, 2015, **15**, 5552–5557.

15 N. Yanai and N. Kimizuka, *Acc. Chem. Res.*, 2017, **50**, 2487–2495.

16 Z. Huang and M. L. Tang, *J. Phys. Chem. Lett.*, 2018, **9**, 6198–6206.

17 Y. Han, S. He and K. Wu, *ACS Energy Lett.*, 2021, **6**, 3151–3166.

18 R. Weiss, Z. A. VanOrman, C. M. Sullivan and L. Nienhaus, *ACS Mater. Au*, 2022, **2**, 641–654.

19 M. W. Brett, C. K. Gordon, J. Hardy and N. J. L. K. Davis, *ACS Phys. Chem. Au*, 2022, **2**, 364–387.

20 M. Wu, D. N. Congreve, M. W. B. Wilson, J. Jean, N. Geva, M. Welborn, T. Van Voorhis, V. Bulovic, M. G. Bawendi and M. A. Baldo, *Nat. Photonics*, 2016, **10**, 31–34.

21 V. Gray, P. Xia, Z. Huang, E. Moses, A. Fast, D. A. Fishman, V. I. Vullev, M. Abrahamsson, K. Moth-Poulsen and M. L. Tang, *Chem. Sci.*, 2017, **8**, 5488–5496.

22 N. Nishimura, V. Gray, J. R. Allardice, Z. Zhang, A. Pershin, D. Beljonne and A. Rao, *ACS Mater. Lett.*, 2019, **1**, 660–664.

23 N. Nishimura, J. R. Allardice, J. Xiao, Q. Gu, V. Gray and A. Rao, *Chem. Sci.*, 2019, **10**, 4750–4760.

24 R. Lai, Y. Sang, Y. Zhao and K. Wu, *J. Am. Chem. Soc.*, 2020, **142**, 19825–19829.

25 L. Hou, A. Olesund, S. Thurakkal, X. Zhang and B. Albinsson, *Adv. Funct. Mater.*, 2021, **31**, 2106198.

26 R. Sun, J. Zang, R. Lai, W. Yang and B. Ji, *J. Am. Chem. Soc.*, 2024, **146**, 17618–17623.

27 W. Liang, C. Nie, J. Du, Y. Han, G. Zhao, F. Yang, G. Liang and K. Wu, *Nat. Photonics*, 2023, **17**, 346–353.

28 L.-H. Jiang, X. Miao, M.-Y. Zhang, J.-Y. Li, L. Zeng, W. Hu, L. Huang and D.-W. Pang, *J. Am. Chem. Soc.*, 2024, **146**, 10785–10797.

29 Z. Y. Huang, C. H. Tung and L.-Z. Wu, *Acc. Mater. Res.*, 2024, **5**, 136–145.

30 C. Mongin, S. Garakyaraghi, N. Razgoniaeva, M. Zamkov and F. N. Castellano, *Science*, 2016, **351**, 369–372.

31 Y. Jiang and E. A. Weiss, *J. Am. Chem. Soc.*, 2020, **142**, 15219–15229.

32 P. B. Green, O. S. Lecina, P. P. Albertini, A. Loiudice and R. Buonsanti, *J. Am. Chem. Soc.*, 2023, **145**, 8189–8197.

33 S. Tamang, C. Lincheneau, Y. Hermans, S. Jeong and P. Reiss, *Chem. Mater.*, 2016, **28**, 2491–2506.

34 D. Rajan, M. Bhaskaran, S. Krishna, A. Thomas and K. G. Thomas, *ACS Energy Lett.*, 2025, **10**, 3700–3728.

35 A. Thomas, K. Sandeep, S. M. Somasundaran and K. G. Thomas, *ACS Energy Lett.*, 2018, **3**, 2368–2375.

36 M. K. Homer, H. C. Larson, G. J. Dixon, E. Miura-Stempel, N. R. Armstrong and B. M. Cossairt, *ACS Nano*, 2024, **18**, 24591–24602.

37 J. R. Heath, *Chem. Soc. Rev.*, 1998, **27**, 65–71.

38 I. N. Chakraborty, S. Roy, G. Devatha, A. Rao and P. P. Pillai, *Chem. Mater.*, 2019, **31**, 2258–2262.

39 I. N. Chakraborty, P. Roy, A. Rao, G. Devatha, S. Roy and P. P. Pillai, *J. Mater. Chem. A*, 2021, **9**, 7422–7457.

40 I. N. Chakraborty, P. Roy and P. P. Pillai, *ACS Catal.*, 2023, **13**, 7331–7338.

41 M. D. Tessier, D. Dupont, K. De Nolf, J. De Roo and Z. Hens, *Chem. Mater.*, 2015, **27**, 4893–4898.

42 Z. Huang and M. L. Tang, *J. Am. Chem. Soc.*, 2017, **139**, 9412–9418.

43 Z. Xu, Z. Huang, T. Jin, T. Lian and M. L. Tang, *Acc. Chem. Res.*, 2021, **54**, 70–80.

44 A. Haefele, J. Blumhoff, R. S. Khnayzer and F. N. Castellano, *J. Phys. Chem. Lett.*, 2012, **3**, 299–303.

45 F. Glaser, C. Kerzig and O. S. Wenger, *Chem. Sci.*, 2021, **12**, 9922–9933.

46 R. Anastasio, W. Peerbooms, R. Cardinaels and L. C. A. van Breemen, *Macromolecules*, 2019, **52**, 9220–9231.